

Spatial and spatio-temporal characterization of movement for the analysis of actions and actors

Leonardo Claudino and Yiannis Aloimonos

Technical Report CS-TR-4995
Department of Computer Science
University of Maryland
College Park, MD, 20740, USA

October 2011

Spatial and spatio-temporal characterization of movement for the analysis of actions and actors

Leonardo Claudino and Yiannis Aloimonos
Department of Computer Science
University of Maryland at College Park
{claudino, aloimonos}@cs.umd.edu

Abstract

Movement data is high-dimensional but often redundant, meaning there is certainly a lower dimensional subspace that spans most of the body configurations within an action performance. We propose that one such representation can be achieved through a decomposition method that explores the existence of key configurations and temporal correlations of those configurations that are typical of action matrices. The approach is compatible with computational models of motor synergies based on matrix factorizations, and it builds upon a method that was earlier proposed in the context of biological motion perception. Our experiments show that vertical jump trials collected from children and young adults can be consistently reconstructed from the resulting representation. We also observe that a subset of that same representation suggests differences among populations of jumpers based on their trials, which serves to illustrate the potential of the method as a tool to analyze both actions and actors.

1 Introduction

Motion capture technology is getting cheaper, more diverse and achieving higher throughput. While raw movement data is very high-dimensional by nature, it is also highly redundant, both at the level of body configurations (e.g. limb positions, postures or joint angles) and the occurrences of such configurations along the timeline of the action; in other words: in both space and time. Therefore, to allow for meaningful computational exploration of hidden patterns of activity, these data must first be shaped into some lower dimensional representation to be manipulated later.

Along these lines, we propose that a suitable compact representation can be obtained by decomposing an action matrix of size T (time instants) \times J (body configurations) with a method that consists of (1) finding a vector space corresponding to key configurations and (2) fitting a mixture model to the projections of the matrix onto each of the individual vectors found, that is, imposing a parametric model to the temporal correlations of each of the body configurations represented by the vectors. Throughout the document, we refer to the computed vector space as the *spatial basis* of the action and we call the parameter set of the mixture model the *spatio-temporal* representation. The approach was tested on optical motion capture data of adults, typically developing children and children with Developmental Coordination Disorder (DCD), all performing vertical jumps. Results suggested it is indeed an adequate action representation for it was observed to allow for proper reconstruction of the jumps and also helped in the inspection of both similarities and differences among populations of jumpers based on their trial distributions. In particular, one of the spatio-temporal parameters presented a clear difference between the distributions of jumps from children with DCD and jumps from typically developing children and adults.

Our work is related to research in computational models of *motor synergies*, more specifically the models involving matrix factorizations. The method we describe builds upon an

existent computational model of *biological motion perception*, proposed by vision psychologists. In the next section, we sketch some of the ideas behind these two related disciplines – one motor, another perceptual – so that the scope of the work is properly situated. In sequence, we formalize the computation of spatial and spatio-temporal representations and present the experiments with the jump data set, along with our main findings.

2 Related work: compact representations in the motor and visual spaces

Synergies, *motor programs* or *action primitives* are only a few of the many ways to denote a hypothetical set of pre-existing modules of effector activation that would be combined by the central nervous system to produce action. Many believe this is the way the brain cuts down dimensionality when controlling and coordinating multiple degrees of freedom in space and time, the so called “Degrees of freedom (DOF) problem” and it came out of the first round of investigations of Bernstein’s work in control and coordination, as once posed by Turvey [1]. This problem has been recently revisited by Latash et al. [2, 3] who discuss the related “principle of abundance”, which refers to the fact that a task demands less degrees of freedom than what is available to be controlled. See Flash et al. [4] for a very interesting summary of findings around the nature of motor primitives at behavioral, muscle, neural, and computational levels. Previous electrophysiological experiments in spinalized animals have indeed presented strong evidence supporting the existence of basic modules of movement that would be additively combined to produce behavior [6]. These modules also seem to be connected to how the same activities are perceived, which is referred by Turvey [1] as “simultaneous organization of afferentiation and efferentiation”. The vast applicability of modeling movement signals based on a compact set of primitives makes the quest for motor synergies an active research topic across many different communities, namely cognitive and humanoid robotics, kinesiology and movement psychology. Theories around the nature of synergies have been proposed in terms of spinal force-fields [6, 7, 8], time-varying muscle forces [9, 10, 11], joint-angle configurations [12], and uncontrolled manifolds [2, 3, 5], among others. Assuming that these action modules actually exist, the way they would be obtained from collected data is still a mystery. The decomposition method that will be covered in the next section has aspects in common with attempts to look for synergies based on matrix factorizations, some of which have been experimented and reported successful in both artificial and real motor data, at least in terms of reconstruction power and consistency of factors and coefficients [13].

Compact representations of movement have also been pursued by vision psychologists while trying to computationally model the visual phenomenon referred to as *biological motion perception* – a term coined to express the ability of humans to perceive moving dots from point-light displays as coherent articulated rigid bodies that give rise to the perception of classes of activities [14, 15, 16]. Of particular relevance, Troje [17] has offered a computational method that produces walking patterns and it is able to discriminate between male and female walks from point-light displays coming from 3-D motion capture positional data. He also breaks up the action analysis into spatial and spatio-temporal representations, although he does not actually use this terminology or address the decomposition in a more general way. The spatial basis described in this paper is analogous to his *eigenpostures*, which represented the 4 first principal components of a single-walker data matrix of dimension $T \times 3J$, with T corresponding to the length of the walk trial (rows) and $3J$

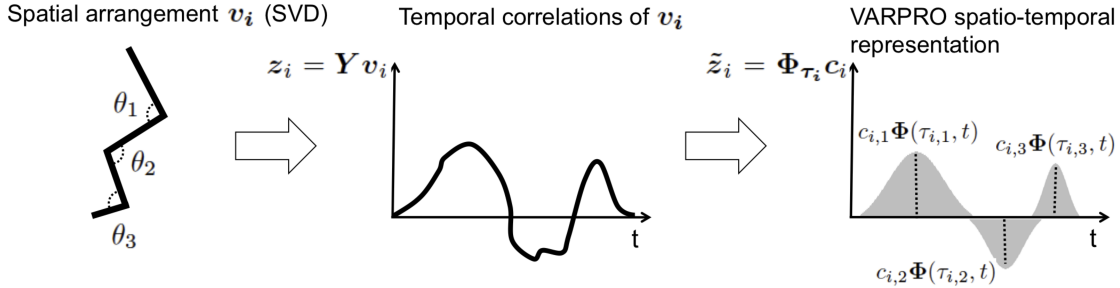


Figure 1: In the example above, J -dimensional spatial basis vector \mathbf{v}_i encodes a linear combination of joint angles θ_1 , θ_2 and θ_3 computed with SVD, as shown by the leftmost figure. The projection $\mathbf{z}_i = \mathbf{Y} \mathbf{v}_i$ of action matrix $\mathbf{Y}_{T \times J}$ onto \mathbf{v}_i results into an often smooth (therefore differentiable) temporal series of correlations that represents the activity of that particular spatial arrangement (posture) along the timeline of the action (center figure). We use VARPRO to produce a compact parametric representation for this temporal behavior by fitting a mixture of $\tilde{\mathbf{z}}_i = \Phi_{\tau_i} \mathbf{c}_i$ to \mathbf{z}_i (right figure) which results in parameter vectors $\tau_i = \{\tau_{i,1}, \tau_{i,2}, \tau_{i,3}\}$ and $\mathbf{c}_i = \{c_{i,1}, c_{i,2}, c_{i,3}\}$. An action matrix is therefore fully characterized by each spatial basis vector \mathbf{v}_i and corresponding set of spatio-temporal parameter vectors τ_i and \mathbf{c}_i . See text for more details.

being the joint- $\{x, y, z\}$ coordinates (columns). He modeled the temporal occurrences of the eigenpostures with a family of sine functions, for which he determined the 4 fundamental frequencies and the relative phases of components 2, 3 and 4 with respect to the first. His sine functions correspond to the basis functions in the spatio-temporal representation presented here.

Troje’s work illustrates that a lower dimensional generative action model is able to both produce the action efficiently and discriminate among performing actors, and his results provided us with the necessary inspiration to re-address his ideas in a more generally applicable model. His choice of modeling the temporal activation of spatial basis vectors as a sum of sinusoids is more suitable to pick patterns that appear throughout the whole timeline of the action but will miss localized events that can reveal coordination differences across populations of performers. Instead, we approach the problem as a matter of fitting a mixture model to the time series and we foster the use of a powerful non-linear least-squares regression tool, Variable Projection or VARPRO [18], which has been used in many different scenarios after almost 40 years of its existence [19], but (to the best of our knowledge) it has not been applied in the context of movement data decomposition. Figure 1 summarizes the decomposition method, which is covered in the next section.

3 Action decomposition

3.1 Computing a spatial basis and spatio-temporal representations

Let $\mathbf{Y}_{T \times J}$ be a multi-dimensional action signal, for example, a T -length sequence of J -joint angle configurations. The k -th order approximation of that signal by SVD, in matrix notation is:

$$\hat{\mathbf{Y}}_{T \times J} = \mathbf{z}_1 \mathbf{v}_1^\top + \mathbf{z}_2 \mathbf{v}_2^\top + \dots + \mathbf{z}_k \mathbf{v}_k^\top,$$

$$\tilde{\mathbf{Y}}(t) \begin{matrix} \boxed{\tilde{\mathbf{Y}}_{T \times J}} \\ \cdots \end{matrix} = \underbrace{\left[\begin{matrix} \boxed{\Phi_{\tau_1}} \\ \Phi_{\tau_1}(t, :) \end{matrix} \times \begin{matrix} \boxed{c_1} \\ \vdots \end{matrix} \right]}_{\tilde{z}_1(t)} \times \begin{matrix} \cdots \\ \mathbf{v}_1^\top \\ \cdots \end{matrix} + \dots + \underbrace{\left[\begin{matrix} \boxed{\Phi_{\tau_k}} \\ \Phi_{\tau_k}(t, :) \end{matrix} \times \begin{matrix} \boxed{c_k} \\ \vdots \end{matrix} \right]}_{\tilde{z}_k(t)} \times \begin{matrix} \cdots \\ \mathbf{v}_k^\top \\ \cdots \end{matrix}$$

Figure 2: Approximating $\mathbf{Y}(t)$ as a linear combination of spatial basis vectors $\mathbf{v}_1, \mathbf{v}_2 \dots \mathbf{v}_k$ (dashed lines), as in Equation 1. Coefficients $\tilde{z}_i(t)$ of each vector \mathbf{v}_i are the product of the t -th time row of its spatio-temporal matrix Φ_{τ_i} and respective linear parameter vector \mathbf{c}_i (solid lines).

where \mathbf{v}_i is one of the top k right singular vectors of \mathbf{Y} , therefore spanning the column (postural) space of that matrix, and projection $\mathbf{z}_i = \mathbf{Y}\mathbf{v}_i$ corresponds to the one-dimensional time series that expresses the correlations of the particular spatial configuration represented by \mathbf{v}_i along the timeline of the action.

For each i , let $\{\Phi(\tau_{i,j}, t) : j = 1 \dots N_i\}$ be a family of N_i Gaussians. Also, let the mean vector $\boldsymbol{\tau}_i = \{\tau_{i,1}, \tau_{i,2} \dots \tau_{i,N_i}\}$ be the only relevant set of parameters, i.e. let the Gaussian functions have fixed standard deviations. Consider Φ_{τ_i} to be the corresponding $T \times N_i$ matrix such that each function is sampled at T instants and it becomes a column of that matrix. We will now model \mathbf{z}_i by fitting a linear combination of the columns of Φ_{τ_i} with linear parameters $\mathbf{c}_i = \{c_{i,1}, c_{i,2} \dots c_{i,N_i}\}$:

$$\tilde{\mathbf{Y}}_{T \times J} = \underbrace{(\Phi_{\tau_1} \mathbf{c}_1)}_{\tilde{z}_1} \mathbf{v}_1^\top + \underbrace{(\Phi_{\tau_2} \mathbf{c}_2)}_{\tilde{z}_2} \mathbf{v}_2^\top + \dots + \underbrace{(\Phi_{\tau_k} \mathbf{c}_k)}_{\tilde{z}_k} \mathbf{v}_k^\top,$$

and we have $\tilde{z}_i = \Phi_{\tau_i} \mathbf{c}_i$. Equivalently, the posture produced by the model at time t is:

$$\tilde{\mathbf{Y}}(t) = \tilde{z}_1(t) \mathbf{v}_1^\top + \tilde{z}_2(t) \mathbf{v}_2^\top + \dots + \tilde{z}_k(t) \mathbf{v}_k^\top, \quad (1)$$

where $\tilde{z}_i(t) = c_{i,1} \Phi(\tau_{i,1}, t) + c_{i,2} \Phi(\tau_{i,2}, t) + \dots + c_{i,N_i} \Phi(\tau_{i,N_i}, t)$. The schema in Figure 2 illustrates how a posture $\mathbf{Y}(t)$ is generated.

Vector \mathbf{v}_i corresponds to the i -th *spatial basis* (SB) vector of action matrix \mathbf{Y} or SB- i . Basis functions $\Phi(\tau_{i,j}, t)$ (and, equivalently, its matrix version Φ_{τ_i}) together with the mean vector $\boldsymbol{\tau}_i$ and the linear parameter vector \mathbf{c}_i constitute what we call the i -th *spatio-temporal representation* (ST) of \mathbf{Y} or ST- i . We are now left with the task of solving for ST- i parameters $\boldsymbol{\tau}_i$ and \mathbf{c}_i .

3.2 Solving for ST- i parameters with VARPRO

Because $\Phi(\tau_{i,j}, t)$ was chosen to be a family of single-parameter Gaussians, this problem turns out to be a separable least-squares regression problem, which allows us to solve for $\boldsymbol{\tau}_i$ and \mathbf{c}_i using variable projection (VARPRO) proposed in the early 1970's by Golub & Pereira [18]. The method exploits the linear substructure of this particular case of nonlinear least squares (NLLS) regression: if you fix the set of non-linear parameters $\boldsymbol{\tau}_i$, the problem turns out to be linear in \mathbf{c}_i and can be solved for the latter using linear least squares (LLS)

technology. In other words, parameter \mathbf{c}_i becomes a function of parameters $\boldsymbol{\tau}_i$ and so, instead of solving:

$$\min_{\boldsymbol{\tau}_i, \mathbf{c}_i} \|\mathbf{z}_i - \tilde{\mathbf{z}}_i(\boldsymbol{\tau}_i, \mathbf{c}_i)\|_2^2,$$

we solve:

$$\min_{\boldsymbol{\tau}_i} \|\mathbf{z}_i - \tilde{\mathbf{z}}_i(\mathbf{c}_i(\boldsymbol{\tau}_i))\|_2^2.$$

Note that this is now a less parametrized problem, a clear advantage of the VARPRO framework. In the LLS stage, the pseudo-inverse solution for \mathbf{c}_i is:

$$\tilde{\mathbf{c}}_i = [\boldsymbol{\Phi}_{\boldsymbol{\tau}_i}]^\dagger \mathbf{z}_i. \quad (2)$$

Recall that $\mathbf{z}_i = \mathbf{Y}\mathbf{v}_i$ is computed by projecting data matrix \mathbf{Y} onto spatial basis vector \mathbf{v}_i computed with SVD, and vector $\tilde{\mathbf{z}}_i$ is the current VARPRO approximation. The solution can be expressed in terms of the truncated SVD of $\boldsymbol{\Phi}_{\boldsymbol{\tau}_i}$:

$$\tilde{\mathbf{c}}_i = \mathbf{V}\tilde{\boldsymbol{\Sigma}}^{-1}\mathbf{U}^\top \mathbf{z}_i. \quad (3)$$

The LLS solution is then directly embedded in the calculation of the Jacobian of the $\tilde{\mathbf{z}}_i(\mathbf{c}_i(\boldsymbol{\tau}_i))$ for the NLLS part of the optimization. As in [20], the Jacobian can be expressed as a sum of two matrices:

$$\mathbf{J} = -(\mathbf{A} + \mathbf{B}), \quad (4)$$

where each of their N_i columns are:

$$\begin{aligned} \mathbf{a}_j &= \mathbf{d}_j \tilde{\mathbf{c}}_i - \mathbf{U}(\mathbf{U}^\top(\mathbf{d}_j \tilde{\mathbf{c}}_i)), \\ \mathbf{b}_j &= \mathbf{V}(\boldsymbol{\Sigma}^{-1}(\mathbf{U}^\top(\mathbf{d}_j^\top \mathbf{r}))). \end{aligned} \quad (5)$$

Here, \mathbf{d}_j is a column vector with the partial derivatives of the j -th Gaussian $\boldsymbol{\Phi}(\tau_{i,j}, t)$ (or the j -th column of matrix $\boldsymbol{\Phi}_{\boldsymbol{\tau}_i}$) w.r.t. its mean $\tau_{i,j}$, evaluated at all time instants t . Matrices \mathbf{U} , $\tilde{\boldsymbol{\Sigma}}^{-1}$ and \mathbf{V} come from the truncated SVD of $\boldsymbol{\Phi}_{\boldsymbol{\tau}_i}$ as in Equation 2. Vector \mathbf{r} is the residual $\mathbf{z}_i - \tilde{\mathbf{z}}_i$. Operations were grouped so that only matrix-vector product multiplications are required, as in O’Leary & Rust [20], who also propose modifications to the way both the partial derivatives and the Jacobian are stored to exploit sparseness. We therefore chose to use their VARPRO implementation in our experiments.

4 Experiments and results

The goals of our experiments were (1) to validate the decomposition approach, by checking whether SB/STB parameters would allow for successful reconstruction of movements performed by different people; (2) to illustrate how the parameters of the model can be used to provide important insights related to both the action and actors involved. Although any kind of action could have been chosen, here we decided to look at *vertical jumps*, a non-trivial behavior that requires strength, coordination and balance.

4.1 Experiment setup and data description

Figure 3 shows the task our subjects performed: participants were instructed to jump vertically as high as possible trying to reach for a visual target. Each vertical jump resulted in a data matrix $\mathbf{Y}_{T \times J}$, of which a single row corresponds to a joint configuration or

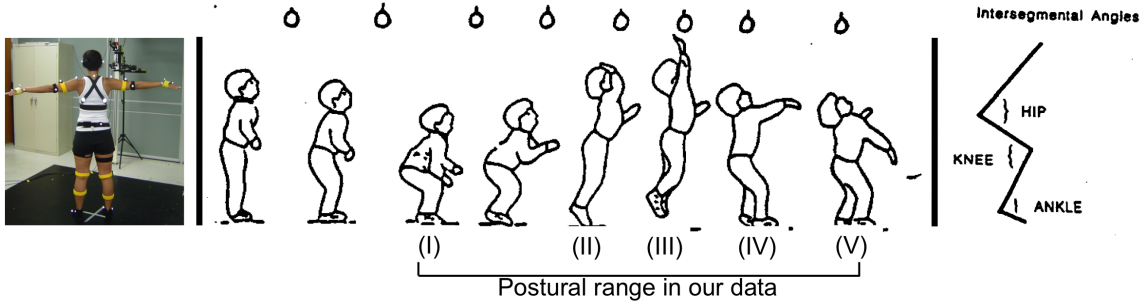


Figure 3: From left to right: subject setup in our lab, vertical jump experiment and intersegmental joint angles used in the experiments. Second and third pictures were adapted from [21].

posture at a certain time. Collected jump trial matrices have $T \approx 80$ rows (about 0.8 seconds) and $J=6$ columns encoding six joints: left and right hips, left and right knees plus left and right ankles. We only used the flexion/extension intersegmental joint angles. The data set described in this section has a total of 343 vertical jumps collected with optical motion capture technology. These jumps come from 4 different populations, totalizing 37 participants: 9 typically developing female children (86 jumps), 6 adult females (61 jumps), 10 typically developing male children (81 jumps), 5 adult males (56 jumps) and 7 children diagnosed with DCD [21] (59 jumps). Children were in the broad age range of 6 to 14 years old. Adults were all in their early 20’s. Trials were manually segmented by an expert in the vertical jump movement, so that they span the same postural range: all poses captured within the initial and final peak knee flexions, as also in Figure 3.

4.2 Vertical jump reconstruction

In our reconstruction experiments, all jump trials were decomposed into a spatial basis of 3 vectors SB- i ($i = \{1, 2, 3\}$) and $N_i=6$ pairs of basis functions/ST parameters τ_i and \mathbf{c}_i for each vector. Standard deviations were fixed as $\sigma_i = \{1/(2 \cdot 1), 1/(2 \cdot 2) \dots 1/(2 \cdot 6)\} \times T$. Note that we do not need to require all N_i to be the same, but we opted to do so in our experiments to simplify the analysis. We refer to these values as N from now on. The reason why we chose $N = 6$ will be clear shortly.

When running VARPRO, means τ_i were constrained to be within $[0, 1]$. This interval corresponds to the time domain of the trial. We also forced linear parameters \mathbf{c}_i to be within $[-1, 1]$ to avoid high fluctuations and ease parameter-based analyses. O’Leary & Rust’s [20] implementation supports constraints to the non-linear parameters since it uses MATLAB[®] `lsqnonlin()` function to solve for those, given the Jacobian of Equations 4 and 5. On the other hand, because their code does not support constraints to the linear parameters, we had to replace the unconstrained pseudo-inverse solution of Equations 2 and 3 with the vector $\tilde{\mathbf{c}}_i$ that minimizes the norm of the residual under the given constraints, or equivalently, $\min_{-1 \leq \tilde{c}_i \leq 1} \|\mathbf{z}_i - \mathbf{U}\tilde{\Sigma}\mathbf{V}^T \tilde{\mathbf{c}}_i\|_2^2$. We chose to use the medium-scale quadratic minimization algorithm of MATLAB[®] `quadprog()` function to find the solution.

Figure 4 shows the statistics of the coefficients of determination R^2 for each individual joint series: the method was able to successfully reconstruct all jumps in the dataset for all

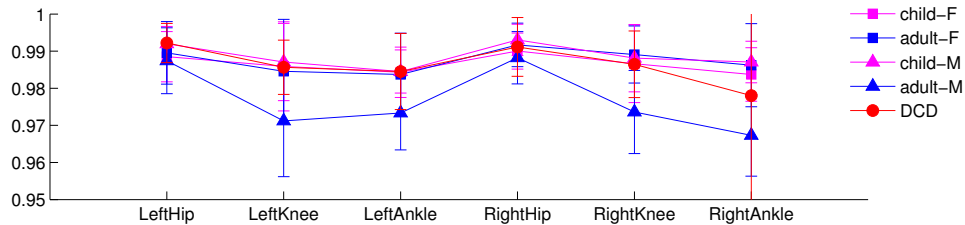


Figure 4: Mean \pm std coefficients of determination R^2 per joint series approximation over all jumps in our dataset, grouped by population. Overall high average coefficients of determination (≥ 0.95) reflect the successful reconstruction ability of the decomposition.

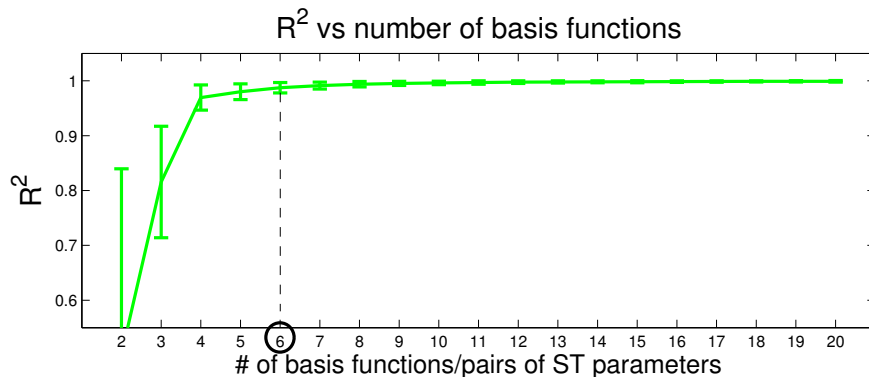


Figure 5: R^2 is plotted against the number of basis functions/pairs of ST parameters. Each point in the plot corresponds to the mean coefficient of determination $R^2 \pm$ std. Here, the coefficient of determination of a trial is itself the average of the coefficients of determination across all joints, since a jump trial is a multi-dimensional time series. A high mean R^2 (good reconstruction) together with a low std (good generalization across trials/populations) reveal $N=6$ to be an adequate trade-off, as circled above.

5 populations considered, with average R^2 not less than 0.95. We also looked at how the reconstruction results are affected by the number of basis functions/pairs of ST parameters N . Figure 5 presents R^2 scores averaged by joints and populations versus $N=\{2 \dots 20\}$. With $N=4$, the method already reaches high reconstruction quality with relatively low variance. We believe the best trade-off between dimensionality and quality of reconstruction is achieved with $N=6$.

4.3 Looking at jumps and jumpers based on the model parameters

From Figure 6, note that spatial basis SB-1 coefficient statistics suggest that over 50% of the (trial-averaged) explained variances in the vertical jump consists of 2 main groups of rotations: hips and ankles (top coefficient values in the range of 0.4 to 0.6) together with knee rotations (bottom coefficients within -0.6 to -0.4). Moreover, overlapping lines show these distributions seem to generalize across all populations examined. In fact, SB-1 works by clustering leg joints into the two existing agonist and antagonist motions, which is also clear from the picture. The same figure also reveals that SB-2 coefficients are al-

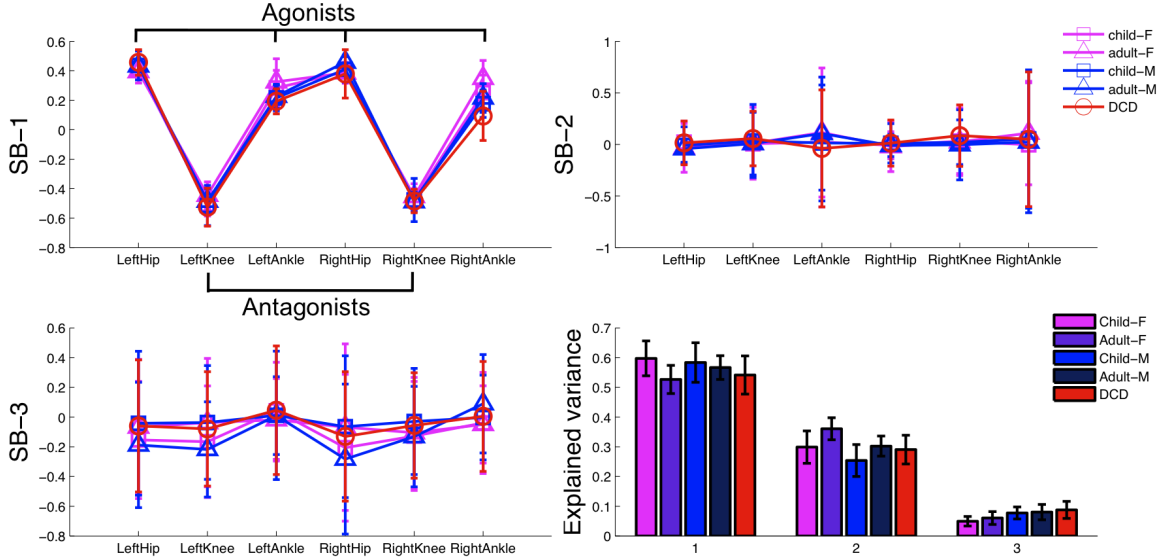


Figure 6: Mean \pm std coefficients of vectors SB-1 (top-left), SB-2 (top-right) and SB-3 (bottom-left). At the bottom right, note that the mean \pm std explained variances per vector are consistent across all populations in the dataset. The distribution of SB-1 coefficients reveals the major component of the vertical jump, apparently common to all populations, which can be noted by the overlapping means and low standard deviations. See text for more details.

most zero-centered and have high variances, in special, left and right ankle coefficients. SB-3 coefficients are also mostly zero-centered, have even higher variances than SB-2 coefficients and less agreement across populations. With average SB-2 and SB-3 coefficients close to zero and no clear interpretation in the context of the jump action, the remaining discussion will focus only on spatio-temporal aspects of SB-1, that is, the statistics of $\tau_1 = \{\tau_{1,1} \dots \tau_{1,6}\}$ and $\mathbf{c}_1 = \{c_{1,1} \dots c_{1,6}\}$ estimated by VARPRO for each of the 6 Gaussians G1 ... G6 of ST-1 (leftmost column of Figure 7). After smoothing all distributions with the MATLAB[®] `ksdensity()` kernel density estimator function, we were able to inspect how these parameters can help to discriminate jumpers of different developmental stages.

When looking at τ_1 distributions, the second column of Figure 7 revealed dominant peaks along $\tau_{1,1}$, $\tau_{1,4}$ and $\tau_{1,6}$, showing that G1, G4 and G6 were somewhat well localized in time, but with significant distribution overlap among populations. Hence these features alone are not very informative about inter-population differences. In particular, for all τ_1 , there were not clear differences between distributions of typically developing children and the ones with DCD. However, we saw differences between adults and children in general: for example, distributions of parameters $\tau_{1,3}$ and $\tau_{1,5}$ were mainly centered at the beginning of the action for adults whereas for children the same parameter distributions were centered once near the middle of the trial and again closer to its end, but with very soft peaks, that is, with high uncertainty. Parameter $\tau_{1,2}$ showed a dominant peak in the adult distribution, close to $t = 0.8$, while children presented very uninformative distributions.

More prominent differences appeared when we instead observed the class distributions of \mathbf{c}_1 (third column of Figure 7), specifically the ones concerning $c_{1,2}$ and $c_{1,6}$, from which

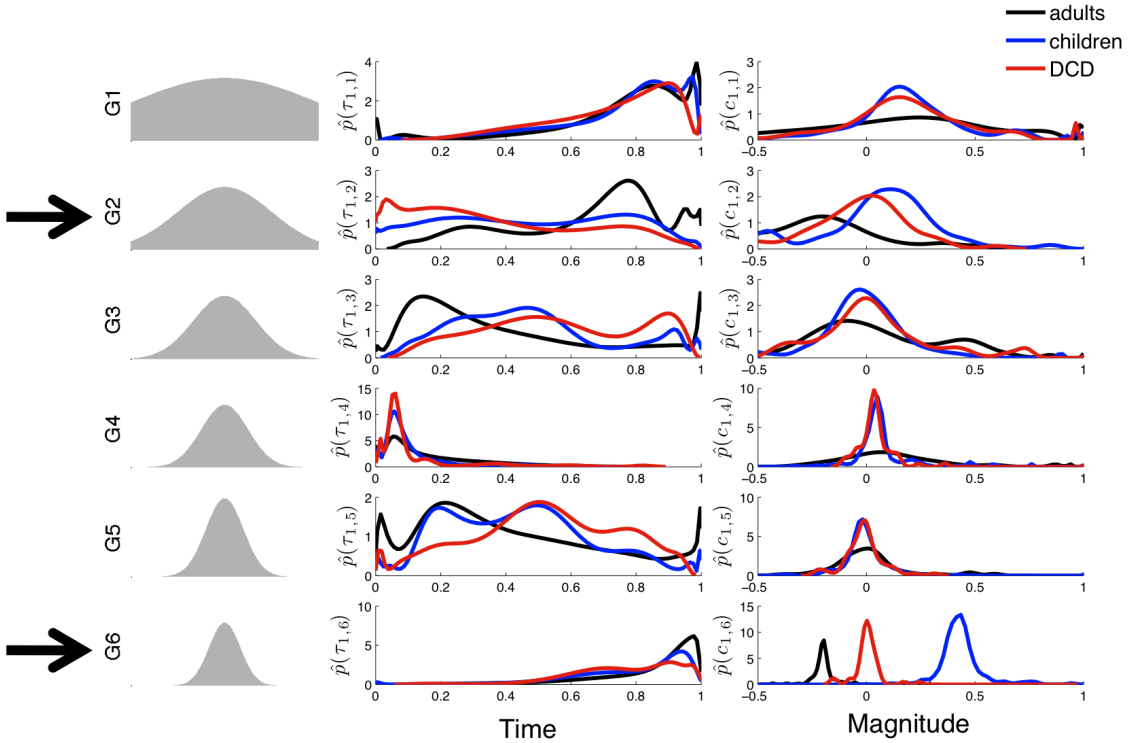


Figure 7: ST-1 parameter statistics for each specific developmental population in our dataset (typically developing children, DCD children and young adults) approximated with a kernel density estimator sampled at 100 points and with a Gaussian smoother kernel. Bandwidth parameters varied across parameter distributions, and were within $[0.01, 0.18]$. Left column: Gaussians that are part of ST-1. Center column: corresponding distributions of means τ_1 . Right column: corresponding distributions of linear parameters c_1 . Arrows indicate that Gaussians G2 and G6 may be able to reveal differences among these populations, as can be noted from the distinct peaks formed along $c_{1,6}$ axis. See text for further discussion.

we saw better defined, bell-shaped distributions for each developmental class. While $c_{1,2}$ showed a high degree of overlap among the curves, $c_{1,6}$ presented a very interesting scenario, with each population sharply peaked at specific magnitude values. In both cases, adults peaked at the negative side, typically developing children peaked at the positive side, and children with DCD were centered at zero. In fact, except for $c_{1,1}$, all distributions of DCD's c_1 were centered at or very close to 0. According to this result, G1 appears to be the most dominant spatio-temporal pattern of SB-1 for this population when DCD jumps are concerned.

By taking into account that the distributions of adults' $\tau_{1,2}$ and $\tau_{1,6}$ peak closer to the end of trial than the children, plus the clear class separation promoted by the corresponding linear parameters $c_{1,2}$ and $c_{1,6}$, we can then conjecture that there are inter-population discrepancies related to the spatial configuration encoded by SB-1 that should be taking place somewhat later in the course of the vertical jump. To discern what exactly these differences mean requires a more thorough investigation and exceeds the scope of this work, but we believe that the framework outlined here would be able to assist in such investigation.

5 Conclusions

This paper describes a decomposition method that breaks the $\mathbf{Y}_{T \times J}$ action data matrix into spatial and spatio-temporal representations. Relevant spatial configurations of joints are identified by SVD and form a spatial basis (SB) for the action. Temporal correlation series of SB vectors, that is, the projection of the data matrix onto SB, are approximated by combinations of Gaussians through a non-linear least-squares regression method, VARPRO. These functions form the basis functions of the spatio-temporal representation (ST) of the action.

Concerning dimensionality, the action matrix is fully described by k (J -dimensional) SB vectors $\mathbf{v}_1, \mathbf{v}_2 \dots \mathbf{v}_k$ plus another $2k$ (N_i -dimensional) ST vectors $\boldsymbol{\tau}_1, \boldsymbol{\tau}_2 \dots \boldsymbol{\tau}_k$ and $\mathbf{c}_1, \mathbf{c}_2 \dots \mathbf{c}_k$, totalizing $kJ + 2k \sum_{i=1}^k N_i$ parameters. Although the number of parameters increases linearly with the number of effectors J , it does not depend directly on the length of the trial. Dimensionality also depends on the number of basis functions/pairs of ST parameters N_i , but these numbers tend to be relatively small: recall that with $N=4$, the method already presented good reconstruction with low inter-trial variance, as in Figure 5.

Based on SB/ST representations, we were able to reconstruct vertical jump trials with high accuracy. The representation was able to generalize over 300 jumps coming from a broad range of jumpers: children from 6-14 years old with and without coordination disorders and young adults. Both genders were represented in the data. We also note that a single SB-1 vector seems to be sufficient to characterize the most important spatial aspect of the jump trials (based on lower-body, intersegmental flexion/extension angles), which helped to narrow down the analysis into 6 spatio-temporal parameters. From the statistics of the means and more importantly the linear coefficients of ST-1, we also determined that populations of jumpers could be reliably discriminated based on our low dimensional analysis of their jumps. Although the results presented here come from a specific case study, we believe the method serves as framework for a variety of movement analyses that can be carried on in the future.

Acknowledgments

This work was supported by NIH grant 5R21DA24323-3. We want to acknowledge Melissa Pangelinan for organizing schedules, recruiting subjects, running them through the test protocol, and taking pictures of the marker setup (e. g. Figure 3). Brad King, for manually labeling key snapshots of each jump trial and sharing his expertise in kinematics and biomechanics of vertical jumps. Dr. Jane Clark, for the relevant references and technical advices. Anne Jorstad and João Soares, for carefully reviewing the manuscript.

References

- [1] Michael T. Turvey, Coordination. *American Psychologist* 45(8):938–953, 1990.
- [2] Mark L. Latash, John P. Scholz and Gregor Schöner, Toward a New Theory of Motor Synergies. *Motor Control* 11:276–308, 2007.
- [3] Mark L. Latash, Mindy F. Levin, John P. Scholz and Gregor Schöner, Motor Control Theories and Their Applications. *Medicina (Kaunas)* 46(6): 382–392, 2010.

- [4] Tamar Flash and Binyamin Hochner, Motor primitives in vertebrates and invertebrates. *Current opinion in neurobiology* 15:660–666, 2005.
- [5] John P. Scholz and Gregor Schöner, The uncontrolled manifold concept: identifying control variables for a functional task. *Exp Brain Res* 126: 289–306, 1999.
- [6] Ferdinando A. Mussa-Ivaldi, Simon F. Giszter and Emilio Bizzi, Linear combination of primitives in vertebrate motor control. *Proceedings of the Natural Academy of Sciences* 91: 7534–7538, 1994.
- [7] Ferdinando A. Mussa-Ivaldi, Nonlinear force fields: a distributed system of control primitives for representing and learning movements. *Proceedings of Computational Intelligence in Robotics and Automation* 84–90, 1997.
- [8] Ferdinando A. Mussa-Ivaldi and Emilio Bizzi, Motor learning through the combination of primitives. *Philosophical Transactions of the Royal Society of London B* 355:1755–1769, 2000.
- [9] Andrea d’Avella and Matthew C. Tresch, Modularity in the motor system: decomposition of muscle patterns as combination of time-varying synergies. *Proceedings of Advances in Neural Information Processing Systems* 14:141–148, 2002.
- [10] Andrea d’Avella, Philippe Saltiel and Emilio Bizzi, Combinations of muscle synergies in the construction of a natural motor behavior. *Nature Neuroscience* 3(6):300–308, 2003.
- [11] Andrea d’Avella, Philippe Saltiel and Emilio Bizzi, Shared and specific muscle synergies in natural motor behaviors. *Proceedings of the National Academy of Science* 8(102):3076–3081, 2005.
- [12] Marco Santello, Martha Flanders and John F. Soechting, Postural Hand Synergies for Tool Use. *The Journal of Neuroscience* 18(23):10105–10115, 1998.
- [13] Matthew C. Tresch, Vincent C. Cheung and Andrea d’Avella, Matrix factorization algorithms for the identification of muscle synergies: evaluation on simulated and experimental data sets. *Journal of Neurophysiology* 95(4):2199–2112, 2006.
- [14] Gunnar Johansson, Visual perception of biological motion and a model for its analysis. *Perception and Psychophysics* 14:201–211, 1973.
- [15] Gunnar Johansson, Spatio-Temporal Differentiation and Integration in Visual Motion Perception. An Experimental and Theoretical Analysis of Calculus-Like Functions in Visual Data Processing. *Psychological Research* 38(4):379–393, 1976.
- [16] Winand H. Dittrich, Action categories and the perception of biological motion. *Perception* 22(1):15–22, 1993.
- [17] Nikolaus F. Troje, Decomposing biological motion: A framework for analysis and synthesis of human gait patterns. *Journal of Vision* 2:371–387, 2002.
- [18] Gene Golub and Victor Pereyra, The differentiation of pseudo-inverses and non-linear least squares problems whose variables separate. *SIAM Journal on Numerical Analysis* 10:413–432, 1973.

- [19] Gene Golub and Victor Pereyra, Separable Nonlinear Least Squares: the Variable Projection Method and its Applications. *Inverse Problems* 19(2):1–26, 2002.
- [20] Dianne P. O’Leary and Bert W. Rust, Variable Projection for Nonlinear Least Squares Problems. *Unpublished manuscript*, 2010, Available at <http://www.cs.umd.edu/users/oleary/software/varpro.pdf>.
- [21] Jody L. Jensen, Sally J. Phillips and Jane E. Clark, For Young Jumpers, Differences Are in the Movement’s Control, Not Its Coordination. *Research Quarterly for Exercise and Sport* 65:258–268, 1994.